JOURNAL OF AIRCRAFT
Vol. 36, No. 1, January–February 1999

Combined Structural and Manufacturing Optimization of Stiffened Composite Panels

Joseph Lynn Henderson,* Zafer Gürdal,† and Alfred C. Loos‡
Virginia Polytechnic Institute and State University, Blacksburg, Virginia 24061

Manufacturing considerations have been incorporated into the design optimization of a blade-stiffened composite panel. For the manufacturing analysis, a one-dimensional resin film infusion model is developed to compute the infiltration time of the resin into a fabric preform of the panel. Results are presented showing the effects of design variables that are important for structural performance, such as cross-sectional geometry variables and material properties, on the panel manufacturing effort. In addition, the effects of manufacturing process variables, such as pressure and temperature, on the structural performance are studied. The structural problem is formulated to minimize the panel mass subject to buckling constraints. A simplified buckling analysis model for the panel is used to compute the critical buckling loads. The objective of the manufacturing problem is to minimize the resin infiltration time. Optimum panel designs for the manufacturing and structures problems alone, as well as for the combined problem, are generated using a genetic algorithm. The results indicate a strong connection between the structural and manufacturing design variables and tradeoffs between the two responses, and illustrate that a multidisciplinary approach to the problem is essential to incorporate manufacturing into the preliminary design stage.

Introduction

ONE of the traditional goals of aircraft structural design is to minimize weight. Laminated composite materials are a natural choice as replacements for metallic structural applications, where high stiffness-to-weight ratios are required. For many aircraft applications, structural panels, such as those encountered in skins, ribs, and spars, are additionally strengthened by stiffening elements. In recent years, the optimal design of composite stiffened panels has been widely studied.[1–4] The optimization process, however, is most often based only on the structural response of the panel. Typically, the objective is to optimize the cross-sectional geometry to minimize the total weight of the panel while satisfying constraints on failure loads based on strength and buckling. In addition to the geometric design variables, laminate stacking sequences in different segments of the panel are also frequently used as design variables.[3–7]

One consideration, however, that has not been addressed in the research just mentioned but arises frequently, particularly for stiffened composite panels, is manufacturing. Geometries that may be optimal from a structural point of view may not lend themselves well to cost-effective manufacturing. In some cases, in fact, the panel geometry may be dictated solely by manufacturing considerations, and/or existing manufacturing techniques. A recent research effort in incorporating cost into the design of composite structures was performed under the NASA Advanced Composite Technology (ACT) program, aimed at the development of low-cost, innovative structural concepts for composite assemblies.[8] A design tool, called COSTADE,[9] has been developed to provide support to designers by projecting the effects of preliminary design decisions on the manufacturing cost and to allow tradeoff studies between the cost and weight of various design configurations prior to concept selection. An important element of cost estimation is the manufacturing plan and the estimation of the cost for each of its process steps. A variety of manufacturing processes are considered in COSTADE, including automated fabric layup and fiber placement, hand layup, resin transfer molding, pultrusion, thermoplastic thermoforming, etc. The cost estimates are based on manufacturing time and resource cost relations that use a set of ground rules for recurring and nonrecurring costs.

Application of the methods of engineering optimization to detailed manufacturing processes is an area that has recently gained considerable attention. The design of dies and processes for injection molding of plastic parts has been a particularly productive area.[10–13] Using design variables that control the dimensions of the dies (and consequently, the geometry of the finished product) along with processing parameters, such as injection pressure and temperature, substantial cost savings could be achieved during fabrication of parts. For example, the optimization strategy used in Ref. 8 was to minimize the injection pressure that helped lower the capital cost of molding equipment as well as reduce the required clamping forces. A constraint on the maximum temperature used for melting was implemented to ensure that material degradation was prevented. A sensitivity analysis for the polymer extrusion process was developed in Ref. 11 and used along with a gradient-based search algorithm for the design of the dies. Minimization of the warpage of injection molded parts was accomplished by designing the wall thickness, as well as process variables such as injection time, postfill cooling and packing times, packing pressure, and melt and coolant temperatures.[12] Optimal placement of injection gate locations was performed in Ref. 13 to improve the quality of plastic parts.

The application of optimization in manufacturing of metallic parts was the topic of a series of recently published papers on metal forming.[14–17] For example, an optimization method for preform die shape design was developed in Ref. 14. The objective of the design was to reduce the difference between the actual final forged shape and the desired final forged shape of a part so that the exact net-shape could be produced. A method

Received Oct. 26, 1997; revision received July 11, 1998; accepted for publication Aug. 9, 1998.

*Graduate Research Assistant, Aerospace and Ocean Engineering; currently Senior Engineer, Boeing Commercial Airplanes, Seattle, WA 98124. Member AIAA.

†Professor, Engineering Science and Mechanics and Aerospace and Ocean Engineering. Associate Fellow AIAA.

‡Professor, Engineering Science and Mechanics.

for designing forging preform shapes based on sensitivity analysis and shape optimization with finite element simulation was performed in Ref. 17. The shapes were designed by including the influence of complex material behavior, which is controlled by strain rate and temperature.

For composite materials, the processes of resin transfer molding (RTM) and resin film infusion (RFI) have recently gained considerable attention for cost-effective fabrication of stiffened composite panels.[18–23] Science-based models for the simulation of the manufacturing processes involved in RTM and RFI have been developed for evaluating the infiltration of resin into a given structural shape such that fully consolidated and void-free parts are obtained.[21–23] However, the primary objective of these models is simply to analyze the manufacturing process for a given composite geometry and set of material properties. With the exception of some effort on the selection of a processing cycle, which involves determination of the temperature and pressure profiles as a function of the manufacturing time, no attempt has been made to optimize the design itself. In fact, as will be postulated in this study, the geometry may have a strong impact on not only the manufacturing technique selected, but also the processing variables involved, which is not addressed in the research cited earlier.

The present paper takes a multidisciplinary approach to the design optimization problem at hand, whereby stiffened composite panels can be generated that not only achieve the desired structural response, but also are easily manufactured. It is also possible that, without much of a penalty in the structural performance, the manufacturing cost of a panel will be reduced substantially by incorporating the appropriate manufacturing analysis and constraints in the design process. To this end, the work presented here seeks to incorporate elements of manufacturing into the design optimization of a blade-stiffened panel. It is desired to observe the effects of structurally important design variables, such as cross-sectional geometry and material properties, on the manufacturing of the panel design. In addition, the less obvious effects of manufacturing process variables, such as pressure and temperature, on the structural performance are studied.

Analyses and Formulation

Elements of Resin Film Infusion

The composites manufacturing process selected to be modeled is that of RFI, which employs a dry textile preform of the part to be manufactured. For complex-shaped parts, such as those commonly found in aircraft structural applications, RFI is a cost-effective manufacturing technique in that its major component processes such as resin impregnation, consolidation, and cure all occur simultaneously. The cure temperature and compaction pressure become the essential parameters in the manufacturing analysis, although, as will be demonstrated later, the geometry of the part to be filled is also important. The basic setup of the RFI process is shown in Fig. 1.

To model RFI, the following processes must be considered simultaneously in the manufacturing analysis: resin flow, resin kinetics, resin viscosity, and preform compaction. The individual processes are then combined to model the RFI process for a one-dimensional representation of a stiffened panel cross section.

The resin infiltration through the preform of the part can be described as flow through a homogeneous porous medium. Assuming that the flow is laminar and that the resin can be treated as an incompressible Newtonian fluid, the infiltration can be expressed by Darcy's law. The one-dimensional differential form of Darcy's law relates q, the flow rate per unit area normal to the flow, to the pressure gradient as

$$q = -\frac{S}{\eta}\frac{\partial P}{\partial z} = \phi\frac{\mathrm{d}z}{\mathrm{d}t} \tag{1}$$

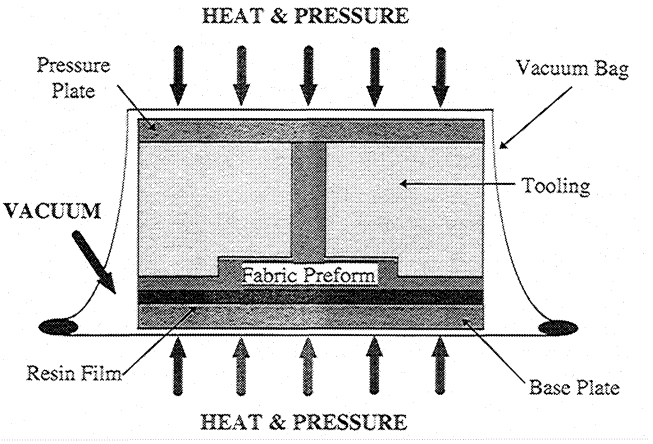

Fig. 1 Basic setup for RFI.

where P is the pressure, S is the permeability of the preform, η is the resin viscosity, and z is the flow direction coordinate (in this case, as will be illustrated later, through-the-thickness of the panel). Equation (1) also shows the relationship between the flow rate and a time-dependent quantity known as the interstitial velocity ($\mathrm{d}z/\mathrm{d}t$). Here, ϕ is the preform porosity and t is the time variable. As will be explained later in the one-dimensional RFI model, integration of Eq. (1) determines the amount of time necessary for the resin to flow a certain distance.

An empirical relation for the resin viscosity (η) is governed by the Williams–Landel–Ferry (WLF) equation[24]

$$\eta(T, \alpha) = \exp\left\{\frac{-C_1[T - T_g(\alpha)]}{C_2 + [T - T_g(\alpha)]} + \ell n[\eta(T_g)]\right\} \tag{2}$$

where T_g is the glass transition temperature, the temperature below which the resin is brittle and glass-like, and C_1 and C_2 are specified constants. Both the glass transition temperature model and the viscosity at T_g, $\eta(T_g)$, are resin-specific, and can both be expressed as polynomial functions of the degree of cure (α)[25]

$$T_g(\alpha) = 283.42 + 196.4\alpha - 925.4\alpha^2 + 3435\alpha^3 - 4715\alpha^4 + 2197\alpha^5 \tag{3}$$

$$\ell n[\eta(T_g)] = 20.72 + 8.56\alpha - 9.69\alpha^2 + 41.17\alpha^3 \tag{4}$$

The values of the constants are also resin-dependent and have the values $C_1 = 29.667$ and $C_2 = 36.926$ for Hercules 3501-6.[22] It is assumed that when the resin viscosity reaches 1000 Pa s, the resin is considered to have gelled, or solidified to the point that flow is no longer possible. It is desired to have the preform completely infiltrated prior to resin gelation. If not, the part will contain voids that will degrade its structural performance.

The resin-curing process involves an exothermic chemical reaction, where a thermosetting resin, like Hercules 3501-6, will form cross links, locking the polymer chains into a three-dimensional lattice structure that cannot be reshaped by heat. Thus, as time progresses, the resin rapidly becomes less fluid and eventually solidifies, producing the desired part. This process is quantified by the degree of cure (α), which is the ratio of the amount of heat evolved during the reaction up to some time t to the total heat of reaction evolved during the entire curing process. Chiou and Letton[25] give the kinetics model for Hercules 3501-6 resin as

$$\frac{\mathrm{d}\alpha}{\mathrm{d}t} = \sum_{i=1}^{3} g_i A_i \exp\left(\frac{-E_i}{RT}\right)(1 - \alpha)^{n_i} \tag{5}$$

where g_i, A_i, and n_i are experimentally determined constants, and E_i are the activation energies, which are also resin-specific. Table 1[22] gives the values of these parameters for Hercules 3501-6. R is the universal gas constant, and T is the temperature at which the resin is cured. Solving Eq. (5) gives α as a function of time, which serves as the input for the viscosity model.

Pressure is necessary to drive the resin into the preform, compact the preform to its required dimensions, and increase the fiber volume fraction by reducing the air pockets left in the preform. The compaction pressure is not only directly tied to the flow rate in Darcy's law, but also indirectly by way of the porosity. The fiber volume fraction (ν_f) of the composite is related to the porosity as follows:

$$\nu_f = 1 - \phi \tag{6}$$

Gutowski et al.[26] developed a relationship between the fiber volume fraction and the compaction pressure. The pressure required for consolidation is written as

$$P = K \frac{\sqrt{(\nu_f/\nu_0)} - 1}{(\sqrt{(\nu_{\max}/\nu_f)} - 1)^4} \tag{7}$$

where ν_0 is the initial fiber volume fraction, $\nu_{\max}$ is the maximum allowable fiber volume fraction that depends on the fiber packing arrangement, and K is a constant based on the fiber material. For AS-4 carbon fibers, $K = 0.159$ kPa, $\nu_0 = 0.51$, and $\nu_{\max} = 0.829$.[26] From the fiber volume fraction, the thickness of an individual ply can be computed as follows:

$$h_{\text{ply}} = \xi/\rho_f \nu_f \tag{8}$$

where ξ is the areal weight of the fiber, and ρ_f is the fiber density. For AS-4 fibers, these values are $\xi = 0.152$ kg/m^2, and $\rho_f = 1.79 \times 10^3$ kg/m^3.

The last element that factors into Darcy's law is the permeability of the preform. Permeability is a measure of the preform resistance to resin flow and is dependent on the fiber radius, the porosity/fiber volume fraction, the packing arrangement of the fibers, and the fiber direction. The permeability along the fiber direction is given by the Kozeny–Carman equation[27]

$$S_{11} = r^2\phi^3/4K_1(1 - \phi)^2 \tag{9}$$

where r is the fiber radius, taken to be 4 μm, and K_1 is a constant with the value of 0.7. The permeability perpendicular to the fibers is computed by Gebart[28] as follows:

$$S_{22} = K_2 r^2(\sqrt{(\nu_{\max}/\nu_f)} - 1)^{5/2} \tag{10}$$

K_2 is a constant with the value of 0.231, and $\nu_{\max}$ is the maximum allowable fiber volume fraction.

One-Dimensional RFI Model

Encompassing the physical processes of RFI discussed earlier, a one-dimensional flow model has been developed to compute the resin infiltration time of a blade-stiffened panel. The panel under consideration is shown in Fig. 2. The panel consists of a skin laminate, and blade and flange laminates, which make up the stiffener. The variables h_s and h_f represent the skin and flange thicknesses, respectively. The blade laminate is in a plane perpendicular to the plane of the skin and flange laminates. Its thickness is represented by w_b. The skin width and the flange width are denoted by w_s and w_f, respectively. For structural applications, several unit cells (Fig. 2) typically comprise the stiffened panel as shown in Fig. 3. The panel carries a total load of F_T and has overall dimensions of $W \times L$.

Table 1 Kinetic parameters for the complex cure reaction of Hercules 3501-6

i	$\ell n\, A_i$, s^{-1}	E_i/R, K	n_i	g_i
1	17.37	11,220	1.06	0.850
2	19.16	10,250	1.17	0.095
3	46.22	20,570	3.05	0.055

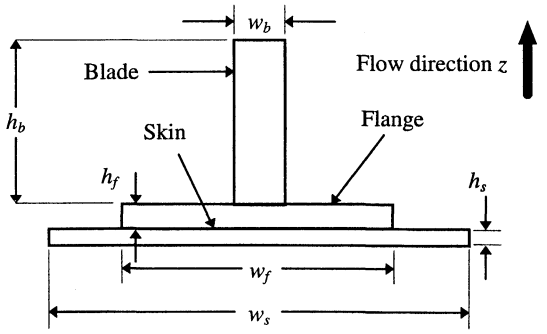

Fig. 2 Stiffened panel cross-sectional geometry.

The skin and blade laminates of the panel are composed of N_s and N_b plies, respectively, of thickness h_{ply}, as determined by Eq. (8). The fiber orientations are assumed to be either 0, $\pm$45, or 90 deg. The 0 deg-fiber direction is along the length of the panel. The skin and blade laminates are also assumed to be symmetric about the midplane and balanced. The flange laminate is obtained by splitting the bottom portion of the blade laminate in half. Thus, the flange thickness (h_f) is one-half of the blade thickness (w_b).

The infiltration time equations for the skin, flange, and blade portions of the panel are developed following the procedure outlined by Cai and Lawrie.[29] It is assumed that the resin flows uniformly such that one-dimensional flow is always maintained. The infiltration times for each panel section are obtained by integrating Darcy's law [Eq. (1)] and applying the continuity equation, which states that the mass flow rate must remain constant throughout the panel. These times for the skin, flange, and blade, respectively, are computed as follows:

$$t_s = \frac{\phi}{PS_s} \int_0^{z_1} \left[\int_0^z \eta(t)\, \mathrm{d}z \right] \mathrm{d}z \tag{11}$$

$$t_f = \frac{\phi}{P} \int_{z_1}^{z_2} \left[\frac{1}{S_s} \int_0^{z_1} \eta(t)\, \mathrm{d}z \frac{w_f}{w_s} + \frac{1}{S_f} \int_{z_1}^{z} \eta(t)\, \mathrm{d}z \right] \mathrm{d}z \tag{12}$$

$$t_b = \frac{\phi}{P} \int_{z_2}^{z_3} \left\{ \left[\frac{1}{S_s} \int_0^{z_1} \eta(t)\, \mathrm{d}z \frac{w_f}{w_s} + \frac{1}{S_f} \int_{z_1}^{z_2} \eta(t)\, \mathrm{d}z \right] \frac{w_b}{w_f} + \frac{1}{S_b} \int_{z_2}^{z} \eta(t)\, \mathrm{d}z \right\} \mathrm{d}z \tag{13}$$

Here, z_1, z_2, and z_3 denote the following through-the-thickness locations in the panel

$$z_1 = h_s, \qquad z_2 = h_s + h_f, \qquad z_3 = h_s + h_f + h_b \tag{14}$$

The skin and flange permeabilities (S_s and S_f) are those perpendicular to the fibers [Eq. (10)]. The blade permeability (S_b), however, is dependent on the stacking sequence and is computed by averaging the permeability of each layer, a method used by Fingerson et al.[23] In the blade, permeability of 0-deg plies is that perpendicular to the fiber direction [Eq. (10)], and for 90-deg plies, it is that in the fiber direction [Eq. (9)]. For $\pm$45-deg plies, it is the average of these two permeabilities. Note that in Eqs. (11–13), the viscosity is left within an integral expression in z because it varies with time, and subsequently, location. In the computation, these integrals are divided into smaller intervals over which the viscosity is taken to be piecewise constant.

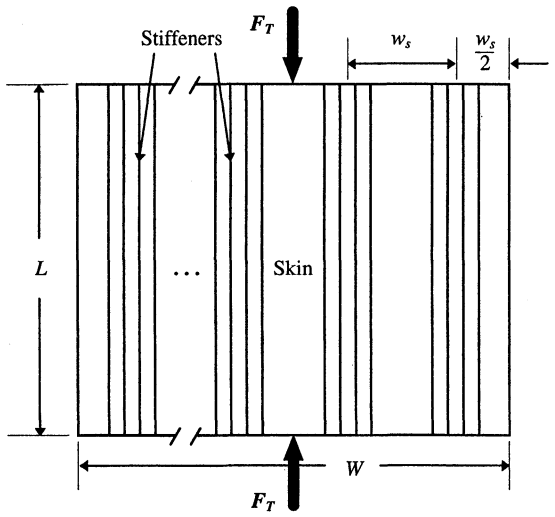

Fig. 3 Planform of panel with multiple stiffeners.

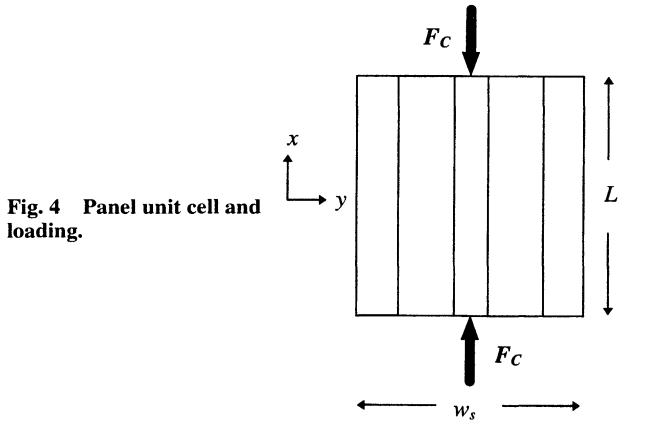

Fig. 4 Panel unit cell and loading.

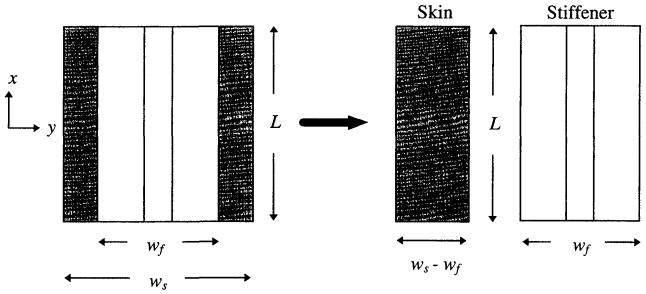

Fig. 5 Skin and stiffener structural elements.

Structural Analysis Model

The planform of the stiffened panel is shown in Fig. 3. For the purposes of structural analysis, a simple unit cell comprised of a stiffener located centrally with respect to a skin segment shown in Fig. 4 is considered. The unit cell is subjected to uniform end-shortening in the x direction, which corresponds to an end load of F_C, and is simply supported along the four edges. This type of loading implies that the skin and stiffener elements deform together along the x direction, and they are assumed to buckle in multiple sinusoidal half-waves in the out-of-plane direction along the length and width of the panel.

The structural criterion in the present work is buckling response of the panel under the prescribed end loading. As will be explained later, design variables that govern the manufacturing process also impact the structural behavior of the panel. One of the goals of this research is to explore the changes in the buckling response of the panel as a function of changes in these design variables. Consequently, a detailed buckling analysis would be prohibitively expensive at this point. Therefore, a simpler approach is taken.

One possible approach to the buckling analysis is to *smear* the engineering properties of the skin and stiffener. However, this method might eliminate some important aspects of the panel's buckling behavior, such as interstiffener buckling. To account for this, the panel is assumed to be composed of two separate structural elements as illustrated in Fig. 5. Here, the skin structural element is the portion of the panel between the flanges of two stiffeners. The stiffener element consists of the blade, flange, and the portion of the skin beneath the flange. Under a uniform end shortening, the applied loading can be distributed as follows:

$$F_{\text{skin}} = \frac{(EA)_{\text{skin}}}{(EA)_{\text{stiff}} + (EA)_{\text{skin}}} F_C$$
$$F_{\text{stiff}} = \frac{(EA)_{\text{stiff}}}{(EA)_{\text{stiff}} + (EA)_{\text{skin}}} F_C \tag{15}$$

where A represents the cross-sectional area and E is Young's modulus. These forces are then compared to the critical loads that will cause each element to buckle as will be discussed later in this paper. To compute the engineering properties of the skin and stiffener, micromechanical principles and classical lamination theory are used.

The structural response of the skin element is computed as a simply supported laminated plate of width $w_f - w_s$, undergoing buckling. Under compression in the x direction, the laminate will buckle into m and n half-waves in the x and y directions, respectively, when the load reaches a critical value given by

$$F_{\text{skin}}^{\text{crit}} = \min_{m,n} \left((w_s - w_f) \left(\frac{\pi L}{m}\right)^2 \left\{ D_{11} \left(\frac{m}{L}\right)^4 + 2(D_{12} + 2D_{66}) \times \left[\frac{mn}{L(w_s - w_f)}\right]^2 + D_{22} \left(\frac{n}{w_s - w_f}\right)^4 \right\} \right) \tag{16}$$

where D_{ij} are the flexural stiffnesses of the skin laminate.

The stiffener element is treated as a simply supported column undergoing axial loading. The critical value of F_{stiff} at which the column will buckle is given by Euler's formula

$$F_{\text{stiff}}^{\text{crit}} = \pi^2 (EI)_{\text{stiff}} / L^2 \tag{17}$$

where I_{stiff} is the moment of inertia of the stiffener cross section, which depends on the stiffener geometry. The stiffener modulus (E_{stiff}) is computed by classical lamination theory, with the laminate used in the calculation combining the stacking sequences of the skin, flange, and blade laminates.

Optimization Problem

Formulation

There are three sets of design variables to be optimized: geometric, material, and manufacturing. The variables are selected as those that impact both the manufacturing and structural response of the panel. The geometric variables define the cross section of the panel, as shown in Fig. 2. These are the skin and blade thicknesses, the skin and flange widths, and the blade height. Note that the panel length (L) remains constant because it has no impact on the one-dimensional manufacturing analysis.

Material variables come in the form of the ply orientation angles, i.e., stacking sequences, of the skin and blade laminates. Both of the laminates are taken to be balanced and symmetric. Because the flange is an extension of one-half of the blade laminate, as previously described, its stacking sequence is also half that of the blade, and thus, is not symmetric. To reduce the number of material variables, the plies are further

arranged into *stacks*, consisting of four plies of the same orientation (a 45-deg stack consists of two +45-deg plies and two −45-deg plies to maintain the balanced condition). The three possible stacks are 0_4, $\pm 45_2$, and 90_4 deg. Thus, for an N-ply symmetric laminate in this work, only $N/8$ stacks have to be considered in the optimization. Previous research[3,4,6,7] employed two-ply stacks for a total of $N/4$ for balanced and symmetric laminates. However, to decrease the total number of design variables, the four-ply stacks are preferred.

The material variables govern the thicknesses of the skin and blade. For N_s and N_b plies in the skin and blade laminates, respectively, the thicknesses are

$$h_s = N_s h_{\text{ply}}, \qquad w_b = N_b h_{\text{ply}} \tag{18}$$

The material variables also affect the structural and manufacturing responses of a panel design. The in-plane properties are dependent on the total numbers of each ply orientation, whereas the stacking sequence itself governs the flexural properties. In addition, the stacking sequence of the blade laminate also determines its permeability as previously discussed.

The manufacturing variables are the compaction pressure and the cure temperature. Pressure not only affects the resin infiltration time, but also the panel's structural response by changing its material properties. Although the compaction pressure has a profound effect on the manufacturing analysis of the panel, preliminary results indicate that it has only a slight effect on the structural performance. In addition, preliminary optimization data reveal that the optimizer will increase the value of P to whatever maximum allowable value it is given. In the actual manufacturing process, however, there are practical limits to the amount of pressure used. For these reasons, pressure is not treated as a design variable. On the other hand, although the cure temperature has no direct impact on structural performance, it plays too large a role in the manufacturing analysis to remain a constant. Variations in cure temperature may lead to premature gelling or curing of the resin before the infiltration process is completed.

The optimization problem includes both continuous and discrete design variables. The geometric and manufacturing variables are continuous, but the stacking sequence optimization is a discrete problem because the ply orientations are limited to three choices. The optimization procedure used must therefore account for this. The optimization problem at hand is a multicriterion one. The structural objective is to minimize the mass of the panel

$$M = LA(W/w_s)(\nu_f \rho_f + \phi \rho_r) \tag{19}$$

where L (0.762 m) is the panel length, A is the total cross-sectional area of the panel, ν_f is the fiber volume fraction, ϕ is the porous volume fraction occupied by the infiltrated resin, and ρ_f (1.79×10^3 kg/m^3) and ρ_r (1.26×10^3 kg/m^3) are the fiber and resin densities, respectively. The mass expression given in Eq. (19) is for a panel consisting of W/w_s stiffeners ($W = 0.812$ m). It is inconsequential for this work if there are a noninteger number of stiffeners. On the manufacturing side, the goal is to minimize the resin infiltration time, the sum of the individual times for each panel section

$$t = t_s + t_f + t_b \tag{20}$$

The constrained optimization problem is stated in Eq. (21)

$$\text{minimize } \psi = \beta_1 M + \beta_2 t$$

$$\text{subject to } \begin{cases} g_1 = (F_{\text{skin}}/F_{\text{skin}}^{\text{crit}}) - 1 = r_{\text{skin}} - 1 \le 0 \\ g_2 = (F_{\text{stiff}}/F_{\text{stiff}}^{\text{crit}}) - 1 = r_{\text{stiff}} - 1 \le 0 \\ g_3 = 0.99 - \Lambda \le 0 \\ g_4 = (w_f/w_b) - 7 \le 0 \\ g_5 = 2 - (w_f/w_b) \le 0 \\ g_6 = (w_f/w_s) - \frac{2}{3} \le 0 \end{cases} \tag{21}$$

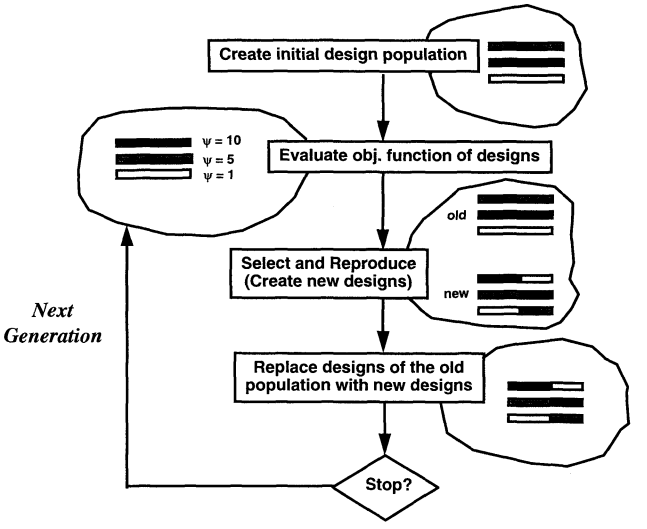

Fig. 6 Genetic algorithm flowchart.

Here, β_1 and β_2 are weighting parameters that govern the relative importance of the individual objectives and are selected to normalize their magnitudes. For the results shown in this paper, these parameters were selected such that each objective had equal weight. The corresponding values of β_1 and β_2 were 0.125 and 0.002, respectively. The structural constraints (g_1 and g_2) state that the actual loading in each element [Eq. (15)] cannot exceed its critical buckling value [Eqs. (16) and (17)]. The manufacturing constraint (g_3) ensures that the preform of the panel be completely filled with resin prior to resin gelation, where Λ is the percentage of the preform filled with resin. The constraint is relaxed to allow 99% and above to be considered completely filled. In addition, constraints are placed on the geometric design variables to restrict the value of the flange width to a range of $2w_b \le w_f \le 7w_b$ (g_4 and g_5), and ensure that space equal to at least $0.5w_f$ remains between individual stiffeners (g_6).

Genetic Algorithms

A genetic algorithm (GA)[30–32] is the optimization method chosen for the problem. The GA is a probabilistic optimization method that works on a population of designs by mimicking the processes of genetic evolution. GAs have several advantages over other optimization procedures. They do not require any derivative information and are insensitive to the complexity of the objective function. For this work, the strongest reason for selecting the GA is its ability to deal with discrete design variables.

Figure 6 is a flow chart of the basic GA. The GA begins with an initial population of Π (50) designs randomly generated. The objective function value for each individual design in the population is evaluated to assess its performance. New designs are created through the processes of selection, crossover, and mutation, and the optimization procedure is repeated until a specified number of generations has passed or after a specified number of generations without any improvement in the objective function value of the best design is reached.

The GA is an unconstrained optimization procedure. Therefore, to incorporate the necessary constraints, a penalty function approach is taken. Penalty functions augment the objective function, and are used in a minimization problem to increase the value of each objective function when constraint violations are encountered. The augmented panel mass (M^*) is given by the following expression:

$$M^* = \begin{cases} \beta_1 M + \chi_1 & \max\ (g_1, g_2), \quad \text{if} \quad g_1 > 0 \quad \text{or} \quad g_2 > 0 \\ \beta_1 M + \varepsilon_1 & \min\ (g_1, g_2), \quad \text{if} \quad g_1 \le 0 \quad \text{and} \quad g_2 \le 0 \end{cases} \tag{22}$$

Here, χ_1 (4.0) is the parameter that penalizes $\beta_1 M$ for constraint violations, and ε_1 (0.005) is a bonus parameter. Both of these quantities are positive. The bonus parameter is used to give a slight advantage to designs that satisfy both of the structural constraints (g_1 and g_2) by reducing their objective function values. The bonus also distinguishes between designs of the same mass, but with different degrees of constraint satisfaction. M^* is further penalized if the geometric constraints (g_4, g_5, and g_6) are not satisfied. This new augmented panel mass is given by

$$M^{**} = M^* + \chi_2 \max(g_4, g_5, g_6, 0) \tag{23}$$

where χ_2 (6.0) is the penalty parameter.

The augmented infiltration time (t^*) is

$$t^* = \beta_2 t + \chi_3 \max(g_3, 0) \tag{24}$$

Again, χ_3 (10.0) is a penalty parameter for designs not satisfying the fill constraint (g_3). Using the two augmented objectives, a new composite objective function (Ψ) can be formed. The unconstrained optimization problem for use with the GA then becomes

$$\text{minimize } \Psi = M^{**} + t^* \tag{25}$$

Results and Discussion

The results presented here will first illustrate the nature of the structural and manufacturing responses of blade-stiffened panel designs and how changing the design variables will impact these responses. To illustrate the motivation behind the multidisciplinary approach to the problem, this section begins with the discussion of optimal panel designs from a previous study.

Table 2 presents the 10 best designs obtained by Nagendra et al.[4] from a study of the weight minimization of a blade-stiffened panel with buckling constraints. The design variables used in that study were the blade height (h_b) and the stacking sequences of the skin and blade laminates. The thicknesses of the laminates were also allowed to vary in stacks of four plies with the total number of plies being N_s and N_b for the skin and blade, respectively. The values of skin width (w_s = 20.30 cm) and flange width (w_f = 6.10 cm) were fixed, and the panels were designed to carry an axial load of 3.50 MN/m and a shear load of 0.876 MN/m. The designs in Table 2, listed in order of increasing panel mass, as obtained by Nagendra et al., were then analyzed by the one-dimensional RFI manufacturing model to compute the time required to fully infiltrate the panels with these geometries. Because the weight minimization problem in Ref. 4 did not require any manufacturing-related variables, values for the applied pressure and temperature must be chosen to perform the manufacturing analysis. Based on preliminary results obtained with RFI model, the pressure and temperature were selected to be 700 kPa and 120°C, respectively. Included in Table 2 are the resin infiltration times (t) and the ranking of the designs in terms of this measure of manufacturing efficiency. The masses (M) given in the table are for panels composed of four stiffener elements, whereas the infiltration time is computed for the unit cell because the manufacturing analysis is one-dimensional.

Table 2 Manufacturing analyses of minimum weight designs from Ref. 4

h_b, cm	N_s	N_b	M, kg	t, s	t, rank
8.03	32	76	10.95	1,181	4
7.72	32	72	10.96	1,012	2
8.09	32	76	10.98	3,225	9
7.75	36	72	10.98	1,249	5
7.89	36	72	11.04	1,275	6
8.06	36	72	11.12	1,474	7
7.72	36	72	11.15	1,174	3
7.74	32	80	11.16	Gelled	10
7.80	40	68	11.16	981	1
7.74	36	76	11.17	1,712	8

From this table, it can be seen that the lightest design only ranks fourth in terms of its infiltration time, whereas the ninth-best structural design ranks first, and therefore, is the design that can be manufactured the fastest. Note that the weight difference between the best and tenth-best designs is only about 2%, whereas there is more than a factor of 3 difference between the lowest and highest infiltration times. Also, note that the resin gels before infiltration is complete in the design ranked tenth. Although no direct relationship between the structural and manufacturing objectives can be made from the data, Table 2 shows that these objectives differ substantially enough to warrant a multiobjective approach to the optimization problem. The results also suggest that it is possible to achieve substantial gains in manufacturing time without much of a loss in structural performance.

The optimization results for the structural problem alone, including the values of the geometric and material variables as well as the results of the structural analysis for a loading of 800 kN and pressure of 700 kPa, are listed next. Geometric variables: skin width (w_s) = 27.82 cm, flange width (w_f) = 6.13 cm, blade height (h_b) = 5.00 cm, skin thickness (h_s) = 0.479 cm, and blade thickness (w_b) = 0.957 cm. Material variables: skin stacking sequence (Θ_s) = $[\pm 45_{10}\ \text{deg}]_s$ and blade stacking sequence (Θ_b) = $[0_{80}\ \text{deg}]$. Manufacturing variables: compaction pressure (P) = 700 kPa and cure temperature (T) = 120°C. Structural analysis: applied loading (F) = 800 kN, panel mass (M) = 7.65 kg, stiffener buckling ratio (r_{stiff}) = 0.983, skin buckling ratio (r_{skin}) = 0.996, flange-to-blade ratio (w_f/w_b) = 6.40, and flange-to-skin ratio (w_f/w_s) = 0.220. Manufacturing analysis: resin infiltration time (t) = 693 s and percentage filled (Λ) = 1.00. The resulting all-zero-ply blade gives the stiffener the maximum stiffness along the loading direction so that it can carry the majority of the load. Meanwhile, the ±45-deg plies keep the skin just under the verge of buckling. The geometric constraints are also both satisfied. In addition, the manufacturing response of the design is assessed with the one-dimensional RFI model. To do this, however, a cure temperature must be selected because it is not a design variable in the structural optimization. As before, a value of 120°C is chosen. The list of structural optimum variables in the previous text shows that the design is fully infiltrated and fills in 693 s.

For the manufacturing optimization, the problem is reformulated because earlier results indicate that the optimizer attempts to reduce the panel to a flat plate of dimensions $W \times L \times h_s$, i.e., the skin. To support the desired loading without buckling, the skin thickness must be allowed to vary. Thus, the number of plies in the skin (N_s) and the cure temperature are the sole design variables. In accordance with the structural optimization results, the stacking sequence of the resulting skin is taken to be of the form $[\pm 45_{Ns/2}\ \text{deg}]_s$, since the permeability of the skin is always that perpendicular to the fibers, regardless of the fiber orientation. The manufacturing optimum for the same pressure (700 kPa) and loading (800 kN) as the structural optimum is shown next: N_s = 116, h_s = 1.39 cm, T = 151°C, r_{skin} = 0.924, M = 14.1 kg, and t = 17.05 s. Note that cure temperature is now a variable and for the manufacturing design has an optimal value of 151°C. In addition, the skin is almost three times thicker than that of the structural optimum. The difference in the objectives will be discussed later.

The combined optimum (P = 700 kPa, F = 800 kN) for the same compaction pressure and loading is given next. Geometric variables: w_s = 27.15 cm, w_f = 6.66 cm, h_b = 5.25 cm, h_s = 0.479 cm, and w_b = 0.957 cm. Material variables: Θ_s = $[\pm 45_{10}\ \text{deg}]_s$ and Θ_b = $[0_{32}\ \text{deg}/90_8\ \text{deg}]_s$. Manufacturing variables: P = 700 kPa and T = 120°C. Structural analysis: F = 800 kN, M = 7.91 kg, r_{stiff} = 0.994, r_{skin} = 0.979, w_f/w_b = 6.95,

and $w_f/w_s = 0.245$. Manufacturing analysis: $t = 498$ s and $\Lambda = 1.00$. Comparing the geometry to that of the structural optimum, it can be seen that the skin is now 2.4% narrower than before, whereas the flange width and blade height have grown by 8.6 and 5.0%, respectively.

The stacking sequence of the skin remains $[\pm 45_{10}\ \text{deg}]_s$ as in the structural optimum because it does not affect the manufacturing analysis. The blade, however, has incorporated two 90-deg stacks into the all-zero structural optimum to reduce its permeability, and thus, reducing its infiltration time. The blade height is increased to 5.25 cm (a 5% increase) compared with the structural optimal design. The addition of 90-deg plies accounts for the increase in the blade height because the stiffener modulus is less than that for the all-zero blade. The stacking sequence is described as $[0_{32}\ \text{deg}/90_8\ \text{deg}]_s$ because the buckling model for the stiffener depends only on the numbers of each ply orientation, not on their order. The resulting stacking sequence given earlier causes the stiffener buckling ratio to approach its critical value, rather than the skin buckling ratio that was the case for the structural optimum. The ratio of flange width to blade thickness is also nearly critical. All other constraints, however, are satisfied with a margin. The panel mass of the combined optimum shown earlier is 3.4% higher than that of the structural optimum, but 44% lower than that of the manufacturing optimum. Comparing the combined optimum infiltration time of 498 s to the 693 s achieved at the same cure temperature of 120°C, approximately a 28% decrease in infiltration time is achieved.

To verify that the design given previously is indeed optimal, the design variables can be perturbed to observe the effects in the structural and manufacturing responses of the panel. The plots that follow demonstrate these resulting tradeoffs in the objective function. The figures show the parametric variation of the infiltration time and the panel mass as a function of various design variables.

For example, Fig. 7 shows the effect of varying the skin width, while keeping the other design variables fixed at their optimal values, on the infiltration time and panel mass. From the figure, it can be seen that increases in w_s decrease both the panel mass and fill time. The ● symbol indicates that the resin has gelled prior to complete infiltration of the preform, and the ○ symbol indicates the largest value w_s can take. The + symbols indicate bounds for buckling constraint satisfaction. The upper bound is where the stiffener buckling ratio is critical, and the lower bound is where the skin buckling ratio is critical. The optimum value of 27.82 cm lies in the middle rather than at the lower bound because of the discrete nature of the genetic algorithm. The plot indicates that the lowest values of the two objectives occurs when $w_s = W$, but both buckling constraints are violated. Thus, the skin width computed by the GA is the optimum.

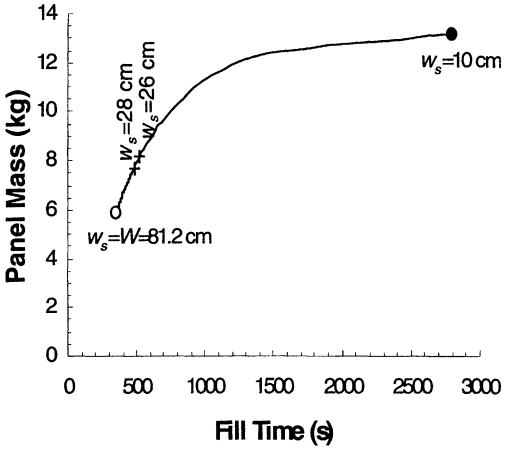

Fig. 7 Objective tradeoff for variable skin width. The ● symbol indicates that the resin has gelled prior to complete infiltration of the preform, and the ○ symbol indicates the largest value w_s can take. The + symbols indicate bounds for buckling constraint satisfaction.

The effect of changing the blade height (see Fig. 8), while keeping the other design variables fixed, on the two objectives is similar to that of the skin width. The smallest infiltration time and panel mass occurs when the h_b shrinks to zero. However, to satisfy both buckling constraints, the height must be at least 5.25 cm, which again was the optimum value given earlier. Arrows are used to indicate the direction of increasing buckling constraint satisfaction.

Varying the flange width, as shown in Fig. 9, produces a different result. This time, the plot indicates an opposition in the objectives. The minimum-mass design occurs when $w_f = 0.14w_s$ ($M = 7.40$ kg). This design also has the largest infiltration time ($t = 2{,}406$ s), and designs with smaller flanges cause the resin to gel prematurely. Moreover, the buckling constraints for this design are violated.

The minimum time design, on the other hand, does satisfy the buckling constraints, and occurs when $w_f = 0.64w_s$ ($t = 299$ s, $M = 9.82$ kg). Above this value, both the mass and time increase. This design, however, violates the geometric constraint that $w_f \leq 7w_b$. Here, $w_f = 19w_b$. The value of w_f that satisfies all of the constraints is $0.245w_s$, giving the optimum design, as previously found, which is 19% lighter than the minimum time design, but fills 67% less quickly. It would appear that relaxing the geometric constraint would give a better design in terms of the manufacturing response, but recall that all other design variables are fixed. Thus, a change in the constraint would affect the outcome of the optimization and the resulting design.

Figure 10 shows that compaction pressure has a common effect on the fill time and panel mass. As with the skin width

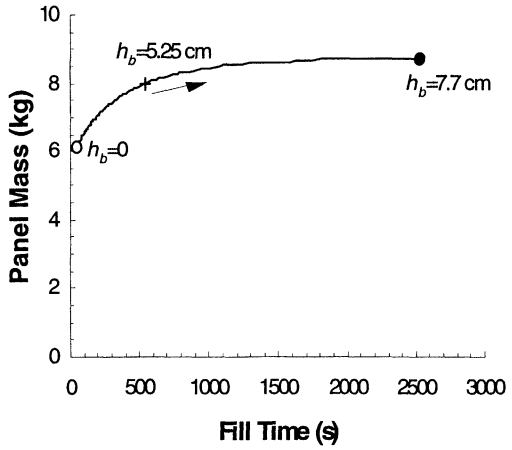

Fig. 8 Objective tradeoff for variable blade height.

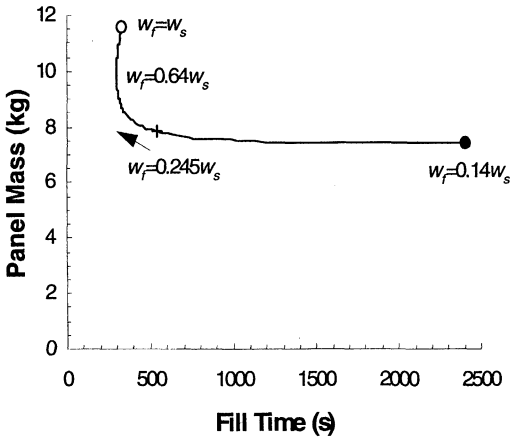

Fig. 9 Objective tradeoff for variable flange width.

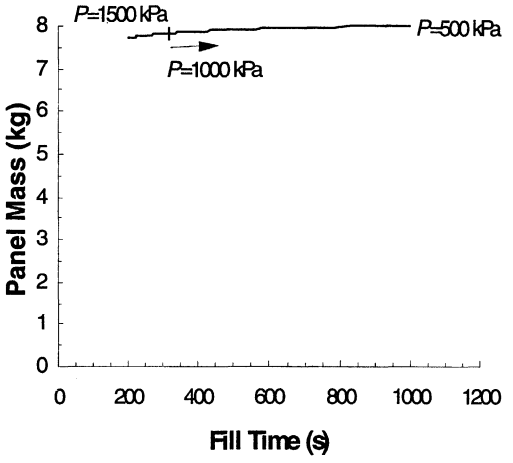

Fig. 10 Objective tradeoff for variable pressure.

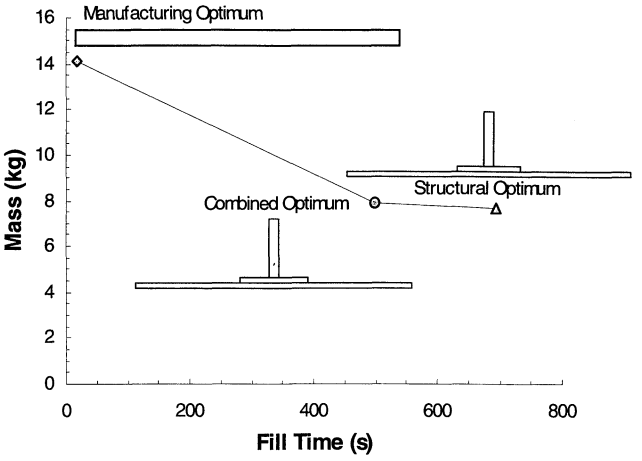

Fig. 11 Manufacturing, structural, and combined optima.

and blade height, increasing the pressure decreases both the structural and manufacturing objectives, although the effect is more pronounced in the time rather than the mass. Note that premature gelation of the resin does not occur over the plotted pressure range, and that the pressure should be below 1000 kPa for the buckling constraints to be satisfied. This is the optimal pressure for the given geometry and cure temperature and yields a time and mass of 307 s and 7.82 kg, respectively. Recall that variations in temperature have no direct impact on the structural response of the panel.

Finally, it is desired to examine the tradeoffs between the structural and manufacturing objectives in the optimal designs previously discussed. Figure 11 plots these optima. The lines connecting the optima are used for illustration purposes. From the figure, it can be seen that the manufacturing optimum has the lowest infiltration time, but also the highest panel mass. The structural optimum, on the other hand, has the highest time, but the lowest mass. The difference in objectives between the manufacturing and structural optima are 98% for the time and 84% for the mass. That is, the manufacturing optimum for the baseline pressure and loading fills 98% faster than the structural optimum for the same case, but is 84% more massive.

The combined optimum, as expected, essentially falls in between the structural and manufacturing optima, but lies closer to the structural design. Going from the structural design to the combined, the panel mass increases. However, compensating for the higher mass, the infiltration time decreases. These results indicate that there is a definite tradeoff between the manufacturing and structural responses in the design of a stiffened composite panel and that a multidisciplinary approach is essential to the optimization problem.

Concluding Remarks

The goal of this research was to integrate manufacturing considerations into the design optimization of a blade-stiffened panel with cross-sectional sizing and process control design variables such as pressure and temperature. Simplified models were developed to determine the panel mass, the critical buckling loads, and the time for resin infiltration as measures of the structural and manufacturing responses. The manufacturing analysis is based on a one-dimensional RFI model, and is capable of accounting for the influence of temperature and pressure on the resin viscosity and curing characteristics that are important for achieving void-free and fully cured composite parts. The manufacturing model is first used to determine the resin infiltration time for a set of designs obtained based on weight minimization only. Results showed a wide range of variation in the infiltration times of panels that weighed practically the same and, hence, the possibility of tradeoffs between structural weight and manufacturing effort.

A GA was used to generate optimum designs for the structures and manufacturing cases alone, as well as for the combined case. The design variables were selected as those that influence both disciplines, and include the cross-sectional geometry, laminate stacking sequences, compaction pressure, and cure temperature. The results presented in this paper demonstrated a strong correlation between structures and manufacturing, confirming that the approach to the problem must be multidisciplinary if manufacturing is to be incorporated into the design process. Using this methodology, it is possible to observe the effects of structurally important design variables, such as geometry, material properties, and laminate stacking sequence, on the manufacturing performance of the panel design, and the less obvious effects of manufacturing process variables, such as pressure and temperature, on the structural performance. For example, compared with the minimum weight design, the combined weight and infiltration time optimum design had 90-deg layers in the stiffener blades (without a change in the blade thickness), which help reduce the infiltration time by about 28%. The loss in the stiffness of the blade was compensated for by increasing the blade height by 5% so that the load-carrying capability of the panel was maintained without violating the buckling constraint. The change in the cross section caused less than 4% weight penalty.

Acknowledgment

This research was sponsored by the Multidisciplinary Analysis and Design Center for Advanced Vehicles at Virginia Tech.

References

[1]Mesquita, L., and Kamat, M. P., "Optimization of Stiffened Laminated Composite Plates with Frequency Constraints," *Engineering Optimization*, Vol. 11, 1987, pp. 77–88.

[2]Nagendra, S., Haftka, R. T., Gürdal, Z., and Starnes, J. H., Jr., "Design of a Blade-Stiffened Composite Panel with a Hole," *Composite Structures*, Vol. 18, No. 3, 1991, pp. 195–219.

[3]Nagendra, S., Haftka, R. T., and Gürdal, Z., "Design of Blade Stiffened Composite Panels by a Genetic Algorithm Approach," *Proceedings of the AIAA/ASME/AHS 34th Structures, Structural Dynamics, and Materials Conference* (La Jolla, CA), AIAA, Washington, DC, 1993, pp. 2418–2436.

[4]Nagendra, S., Jestin, D., Gürdal, Z., Haftka, R. T., and Watson, L. T., "Improved Genetic Algorithm for the Design of Stiffened Composite Panels," *Computers and Structures*, Vol. 58, No. 3, 1996, pp. 543–555.

[5]Haftka, R. T., and Walsh, J. L., "Stacking Sequence Optimization for Buckling of Laminated Plates by Integer Programming," *AIAA Journal*, Vol. 30, No. 3, 1992, pp. 814–819.

[6]Le Riche, R., and Haftka, R. T., "Optimization of Laminate Stacking Sequence for Buckling Load Maximization by Genetic Algorithm," *AIAA Journal*, Vol. 31, No. 5, 1993, pp. 951–956.

[7]Henderson, J. L., "Laminated Plate Design Using Genetic Algorithms and Parallel Processing," *Computing Systems in Engineering*, Vol. 5, 1994, pp. 441–453.

[8]Freeman, W. T., Vosteen, L. F., and Siddiqi, S., "A Unified Approach for Composite Cost Reporting and Prediction in the ACT Program," NASA CP-3104, 1991.

[9]Mabson, G. E., Ilcewicz, L. B., Graesser, D. L., Metschan, S. L., Proctor, M. R., Tervo, D. K., Tutle, M. E., and Zabinsky, Z. B., "Cost Optimization Software for Transport Aircraft Design Evaluation (COSTADE)—Overview," NASA CR-4736, Aug. 1996.

[10]Turng, L. S., Chiang, H. H., and Stevenson, J. F., "Optimization Strategies for Injection Molding," *Society of Plastics Engineers Annual Technical Conference*, Society of Plastics Engineers, Brookfield, CT, 1995, pp. 668–672.

[11]Smith, D. E., Tortorelli, D. A., and Tucker, C. L., III, "Optimal Design of Polymer Sheeting Dies," *Society of Plastics Engineers Annual Technical Conference*, Society of Plastics Engineers, Brookfield, CT, 1995, pp. 42–46.

[12]Lee, B. H., and Kim, B. H., "Optimization of Part Wall Thicknesses to Reduce Warpage of Injection-Molded Parts Based on the Modified Complex Method," *Polymer-Plastics Technology Engineering*, Vol. 34, No. 5, 1995, pp. 793–811.

[13]Pandelidis, I., and Zou, Q., "Optimization of Injection Molding Design, Part I: Gate Location Optimization," *Polymer Engineering and Science*, Vol. 30, No. 15, 1990, pp. 873–882.

[14]Zhao, G., Wright, E., and Grandhi, R. V., "Preform Die Shape Design in Metal Forming Using an Optimization Method," *International Journal for Numerical Methods in Engineering*, Vol. 40, No. 7, 1997, pp. 1213–1230.

[15]Han, C. S., Grandhi, R. V., and Srinivasan, R., "Optimum Design of Forging Die Shapes Using Nonlinear Finite Element Analysis," *AIAA Journal*, Vol. 31, No. 4, 1993, pp. 774–781.

[16]Zhao, G., Wright, E., and Grandhi, R. V., "Computer Aided Preform Design in Forging Using the Inverse Die Contact Tracking Method," *International Journal of Machine Tools and Manufacture*, Vol. 36, No. 7, 1996, pp. 755–769.

[17]Wright, E., and Grandhi, R. V., "A Shape Optimization Technique for Controlling Deformation Parameters in Forging," AIAA Paper 97-1113, April 1997.

[18]Robertson, F. C., "Resin Transfer Moulding of Aerospace Resins—A Review," *British Polymer Journal*, Vol. 20, 1988, pp. 417–426.

[19]Coulter, J. P., Smith, B. F., and Güçeri, S. I., "Experimental and Numerical Analysis of Resin Impregnation During the Manufacturing of Composite Materials," *Proceedings of the 2nd Technical Conference of the American Society for Composites*, Technomic Publishing Co., Inc., Lancaster, PA, 1987, pp. 209–217.

[20]Li, S., and Gauvin, R., "Numerical Analysis of the Resin Flow in Resin Transfer Molding," *Journal of Reinforced Plastics and Composites*, Vol. 10, 1991, pp. 314–327.

[21]Weideman, M. H., Loos, A. C., Dexter, H. B., and Hasko, G. H., "An Infiltration/Cure Model for Manufacture of Fabric Composites by the Resin Infusion Process," Virginia Tech Center for Composite Materials and Structures, Virginia Polytechnic Inst. and State Univ., CCMS-92-05, Blacksburg, VA, 1992.

[22]MacRae, J. D., Loos, A. C., Dexter, H. B., Deaton, J. W., and Hasko, G. H., "Development and Verification of a Resin Film Infusion/Resin Transfer Molding Simulation Model for Fabrication of Advanced Textile Composites," Virginia Polytechnic Inst. and State Univ., VPI-E-94-09, Blacksburg, VA, 1994.

[23]Fingerson, J. C., Loos, A. C., and Dexter, H. B., "Verification of a Three-Dimensional Resin Transfer Molding Process Simulation Model," Virginia Polytechnic Inst. and State Univ., VPI-E-95-04, Blacksburg, VA, 1995.

[24]Ferry, J. D., *Viscoelastic Properties of Polymers*, 2nd ed., Wiley, New York, 1970.

[25]Chiou, P., and Letton, A., "Reaction Kinetics and Chemoviscosity of a Thermoset Exhibiting Complex Curing Behavior," *4th American Society for Composites Technical Conference*, Technomic Publishing Co., Inc., Lancaster, PA, 1989, pp. 157–166.

[26]Gutowski, T. G., Cai, Z., Bauer, S., Boucher, D., Kingery, J., and Wineman, S., "Consolidation Experiments for Laminate Composites," *Journal of Composite Materials*, Vol. 21, No. 7, 1987, pp. 650–669.

[27]Carman, P. C., "Fluid Flow Through Granular Beds," *Transactions, Institution of Chemical Engineers*, Vol. 15, 1937, pp. 150–166.

[28]Gebart, B. R., "Permeability of Unidirectional Reinforcements for RTM," *Journal of Composite Materials*, Vol. 26, 1992, pp. 1100–1133.

[29]Cai, Z., and Lawrie, D. J., "A Simplified Mold Filling Program for the RTM Process," 24th International SAMPE TC, Oct. 1992.

[30]Haftka, R. T., and Gürdal, Z., *Elements of Structural Optimization*, 3rd Revised and Expanded Edition, Kluwer, Dordrecht, The Netherlands, 1992.

[31]Goldberg, D. E., *Genetic Algorithms in Search, Optimization, and Machine Learning*, Addison–Wesley, Reading, MA, 1989.

[32]Davis, L. (ed), *Handbook of Genetic Algorithms*, Van Nostrand Reinhold, New York, 1991.